Role of surface roughness in hysteresis during adhesive elastic contact

Haneesh Kesari[a]; Joseph C. Doll[a]; Beth L. Pruitt[a]; Wei Cai[a]; Adrian J. Lew[a]

[a] Department of Mechanical Engineering, Stanford University, Stanford, CA 94305-4040, USA

PLEASE SCROLL DOWN FOR ARTICLE

Role of surface roughness in hysteresis during adhesive elastic contact

Haneesh Kesari, Joseph C. Doll, Beth L. Pruitt, Wei Cai
and Adrian J. Lew*

*Department of Mechanical Engineering, Stanford University,
Stanford, CA 94305-4040, USA*

In experiments that involve contact with adhesion between two surfaces, as found in atomic force microscopy or nanoindentation, two distinct contact force (P) versus indentation-depth (h) curves are often measured depending on whether the indenter moves towards or away from the sample. The origin of this hysteresis is not well understood and is often attributed to moisture, plasticity or viscoelasticity. Here we report experiments which show that hysteresis can exist in the absence of these effects, and that its magnitude depends on surface roughness. We develop a theoretical model in which the hysteresis appears as the result of a series of surface instabilities, in which the contact area grows or recedes by a finite amount. The model can be used to estimate material properties from contact experiments even when the measured P–h curves are not unique.

Keywords: atomic force microscopy; nanoindentation; surface roughness; adhesion; contact mechanics

1. Introduction

Adhesive contacts play a central role in many biological phenomena and engineered systems, such as in cell adhesion [1] and microdevices [2]. In particular, characterization of materials using contact experiments, such as Atomic Force Microscopy (AFM), requires an understanding of adhesive contacts [3–5]. During adhesive contact, the measured contact force versus indentation-depth ($P-h$) curves often display a clear and repeatable hysteresis loop, $\mathcal{H}$ [4,6–9] (Figure 1a). These curves have two branches, one measured as the indenter moves towards the sample, and another one as it moves away. The area inside measures the energy loss during a cycle. In some adhesive contact experiments (such as [4,6–9] and this study), $\mathcal{H}$ depends on the maximum indentation-depth, $|h_{\min}|$. We refer to this behavior as depth-dependent hysteresis (DDH).

DDH cannot be explained by classical contact theories [10–13], which predict a P–h curve with a single branch in the regime of $h < 0$. Fitting experimental data displaying DDH to these theories leads to different estimates for material properties depending on which branch of the curve is used [8,9,14,15]. The mechanism of DDH

---

*Corresponding author. Email: lewa@stanford.edu

is not well understood, but it has been attributed to several factors, such as material damage (plasticity) [16], ambient moisture [6,17], viscoelasticity [18], and chemistry-related mechanisms [7–9,19]. Here, we report experiments in which the observed DDH cannot be explained by these factors alone. Furthermore, the observed DDH is found to depend on surface roughness. Thus, we hypothesize that surface roughness coupled with adhesion can give rise to DDH. We also present a model for adhesive elastic contact between rough surfaces whose predictions are consistent with our experiments. Most notably, it predicts different *P–h* branches during loading and unloading. Therefore, our model enables the estimation of material properties by simultaneously fitting both branches of the experimental *P–h* curves, instead of having to choose among the two. The fitting also provides certain information about surface roughness of the contacting surfaces.

2. Materials and methods

2.1. *Hysteresis measurements*

To investigate the mechanism of DDH, we measured *P–h* curves on four polydimethylsiloxane (PDMS) samples having varying roughness using both AFM and nanoindentation (NI) apparatus. The AFM tip was a spherical glass bead and the NI tip was a flat face of a truncated diamond cube. Details of PDMS sample preparation, AFM, and NI experiments are given in the following sections.

On each sample we measured *P–h* curves at five different sample spots that were separated from one another by at least 200 μm. We brought the tip into contact with each sample spot several times ($\approx$20); each time starting from a tip-sample separation where $P = 0$. The tip base was moved towards the samples until the tip was pushed into the sample by a predetermined amount – $|h_{min}|$ – and then moved away until $P = 0$ again. We counted each time the tip is brought into contact with the sample as a contact cycle. The speed of the tip's base (d) was kept constant during the measurements. As stated, at each sample location we performed several contact cycles with $|h_{min}|$ ranging from 0 to 1500 nm. For each $|h_{min}|$, we calculated the energy loss $\mathcal{H}$ by computing the area enclosed within the corresponding contact cycle's *P–h* loop.

For a given $|h_{min}|$, the $\mathcal{H}$ for a sample is the average of the data taken at the five locations. The error bars for $\mathcal{H}$ are the standard deviation of the data taken over the five locations.

2.2. *PDMS sample preparation*

We fabricated PDMS samples having varying roughness but identical mechanical properties and surface chemistry using a soft-lithography technique [20], where the same PDMS solution (base:crosslinker = 10:1, Sylgard 184, Dow Corning, Midland, MI) was cast onto different silicon (Si) molds (University Wafer, South Boston, MA). The Si molds were roughened to varying extents by exposing them to reactive ions in a parallel plate plasma etcher (RIE-100, Drytek) for durations

ranging from 30 s to 6 min. The gas flow rates ($SF_6/O_2 = 90/25$ sccm), RF power (200 W), and pressure (70 mTorr) were held constant for all etches. The PDMS solution was mixed well and deaerated in a centrifugal mixer (AR-100, Thinky, Tokyo, Japan) to obtain a uniformly mixed prepolymer solution. The Si molds were vapor coated with a releasing agent (Chlorotrimethylsilane, Sigma-Aldrich, St. Louis, MO) before casting a 5–10 mm thick prepolymer solution onto them. Vacuum was applied to the casts for 15 min before curing them at room temperature ($\approx 20°C$) for 48 h.

We measured the Si molds topography by scanning their surfaces using a sharp Si-tipped AFM operated in tapping mode. We performed these measurements over $4 \mu m^2$ scan areas at three different locations on each sample. From these measurements, we observed that the Si molds root mean square (RMS) roughness varied from 0.65 to 1.52 nm. The number of asperities, which we determined by counting the points where the topography had a local maxima, were 213 ± 10, 99 ± 8, 98 ± 8, and 75 ± 4 per square micron on the Si wafers exposed to 0 s, 30 s, 3 min, and 6 min of reactive ion etching, respectively.

Because of the large compliance of PDMS (Young's modulus ~ 1 MPa), we could not measure the PDMS sample roughness directly using an AFM. However, the soft-lithography technique we used [20] is known to replicate features down to 2 nm [21]. Thus, in this work we assume that the RMS roughness of our PDMS samples is proportional to that of their respective Si molds on which they were cast. Furthermore, since the different PDMS samples were cast from the same prepolymer solution we expect that all samples have the same bulk mechanical properties and surface chemistry.

2.3. *AFM contact experiments*

Indentation with soda lime glass beads (Duke Scientific, Palo Alto, USA) was performed in air at room temperature using an AFM (alpha300A, Witec Instruments, Ulm, Germany) operated in the contact mode. The beads had a diameter of 50 μm, and an RMS roughness of 6 nm. They were attached onto an AFM cantilever (Arrow NCR, Nanoworld, Neuchâtel, Switzerland) using epoxy resin. The spring constant of the cantilever was estimated to be 30 ± 6 N/m by measuring the resonant frequency, for details see [22].

Underwater measurements were performed by placing the samples in a container filled with deionized water. At the beginning of the experiment the AFM tip was lowered into the container such that it was completely under water.

2.4. *NI experiments*

To estimate the viscoelasticity of our PDMS samples, we also measured *P–h* curves on all our PDMS samples using a flat faced diamond tip. These measurements were performed using a NI apparatus (Hysitron, Minneapolis, USA). The tip is a corner of a diamond cube whose apex has been flattened. The RMS roughness of the

diamond tip measured through imprints on gold surfaces was <1 nm. The flat contacting face is an equilateral triangle with sides 10.5 μm long and an area of 47 μm². The machine was operated in displacement control mode.

3. Results and discussion

3.1. *AFM experiments*

Figure 1a shows the *P–h* curves using an AFM during glass-PDMS contact at the loading rate $\dot{d} = 10$ nm/s. Two distinct *P–h* branches are found for the loading and unloading stages. Figure 1b shows that the energy loss $\mathcal{H}$ of a contact cycle increases with $|h_{min}|$, which is a signature of DDH. Figures 1c and d show that similar behavior is also observed at a faster loading rate of $\dot{d} = 1000$ nm/s. For a given $|h_{min}|$, the energy loss is larger at the higher loading rate. This rate dependence will be discussed further in Section 3.2.

At the higher loading rate of $\dot{d} = 1000$ nm/s, we measured the energy loss as a function of $|h_{min}|$ on PDMS samples with different surface roughness but similar bulk properties and surface chemistry (see Section 2.2). We chose to use the higher loading rate in order to expedite the experiments and reduce any instrumentation drift errors in our measurements. Figure 1d shows that for a given $|h_{min}|$, $\mathcal{H}$ increases as the sample RMS roughness grows from 0.65 to 1.31 nm, but then decreases as RMS roughness increases further to 1.52 nm. These data are also plotted in Figure 2a with RMS roughness as the *x*-axis. This behavior of initial increase and then decrease of $\mathcal{H}$ with RMS roughness was observed using two different sets of PDMS samples, AFM cantilevers, and glass beads on two different days. The two sets of PDMS samples were prepared using the same set of Si molds.

Ambient moisture can cause DDH because condensation of a liquid meniscus at the contact periphery is known to change the contact forces [23, p. 880]. To test this possibility, we performed glass bead-PDMS contact experiments under water, where no meniscus can form. Figures 1e and f show that DDH still appears in this experiment. We estimated the contributions to DDH from water's viscosity to be negligible (∼attojoules) for the loading rates used in our experiments. This is confirmed by the flat region of the *P–h* curve in Figure 1e at $h > 0$, which indicates that no appreciable force was measured while the cantilever moves in water before touching the sample. Hence, we expect that the same mechanisms causing DDH in the in-air experiments are responsible for DDH in the under water experiments as well. In addition, moisture contribution in our in-air AFM experiments, shown in Figures 1a–d, should be negligible since PDMS is known to be hydrophobic [24], and these experiments were performed at conditions (relative humidity 34%, temperature 23°C) at which moisture condensation is estimated to be negligible. Hence, we can rule out the possibility of moisture as the main cause of DDH in the experiments shown in Figure 1.

To test the possibility that the observed DDH may be instrumentation artifacts, we performed glass-on-glass indentation experiments both before and after the in-air and under-water glass-PDMS experiments. No sign of DDH was observed in the
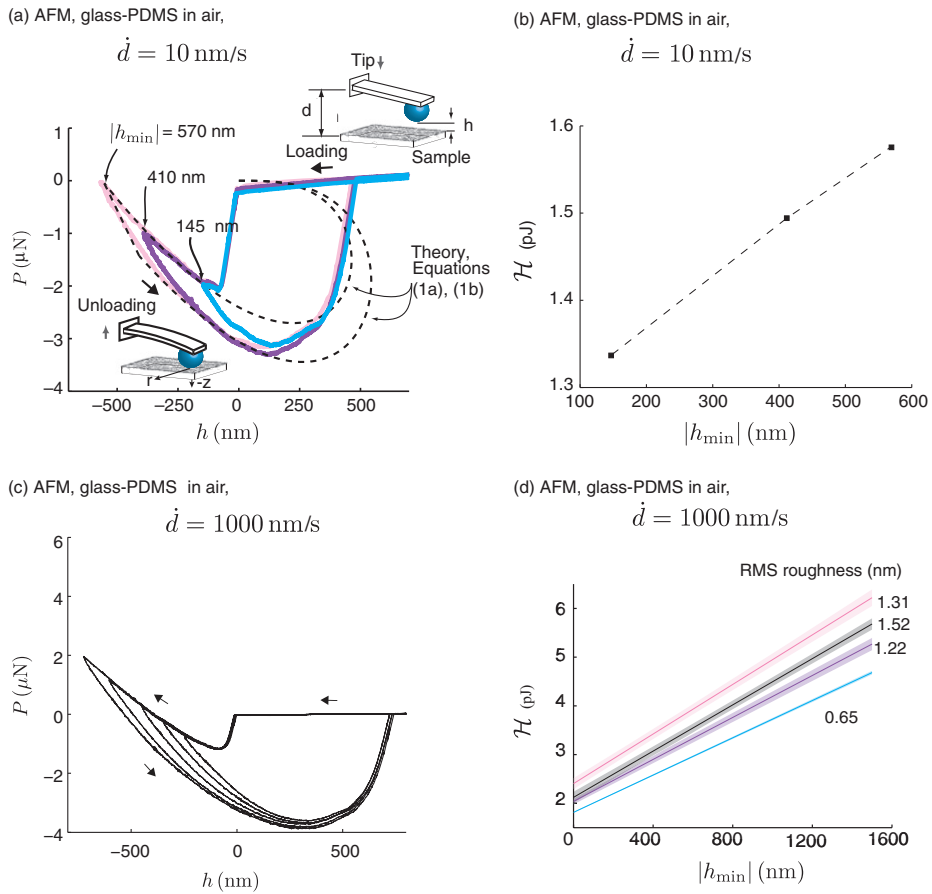
(a) AFM, glass-PDMS in air, $\dot{d} = 10\,\text{nm/s}$

(b) AFM, glass-PDMS in air, $\dot{d} = 10\,\text{nm/s}$

(c) AFM, glass-PDMS in air, $\dot{d} = 1000\,\text{nm/s}$

(d) AFM, glass-PDMS in air, $\dot{d} = 1000\,\text{nm/s}$

Figure 1. (a) AFM contact force (P) as a function of indentation-depth (h) during glass-PDMS contact in air at an indenting rate of $\dot{d} = 10\,\text{nm/s}$. The PDMS sample was cast on a Si wafer with an RMS roughness of 1.31 nm. The dashed lines in (a) are the P–h curves predicted by Equations (1a) and (1b). (b) The energy loss $\mathcal{H}$ as a function of the $|h_{\min}|$ obtained from the P–h curves shown in (a). (c) AFM P–h curve during glass-PDMS contact in air at $\dot{d} = 1000\,\text{nm/s}$. The PDMS sample was cast on a Si wafer with an RMS roughness of 0.65 nm. (d) The energy loss $\mathcal{H}$ as a function of $|h_{\min}|$ for indentation conditions similar to (c) on several PDMS samples cast on Si wafers with different RMS roughness (indicated next to each curve). Each curve corresponds to a different PDMS sample and was computed from measurements at five different locations on the sample. The shaded region around each curve indicates the standard deviation of the measurements taken at five locations on the PDMS samples. At each location $\mathcal{H}$ was measured for ≈ 20 different $|h_{\min}|$, for additional details see Section 2.1. (e) AFM P–h curve during glass-PDMS contact under water at $\dot{d} = 1000\,\text{nm/s}$. The PDMS sample was cast on a Si wafer with an RMS roughness of 0.65 nm. (f) The energy loss $\mathcal{H}$ as a function of $|h_{\min}|$ obtained from (e).

glass-on-glass experiments, which rules out instrumentation artifacts as a cause of the observed DDH. Furthermore, successive P–h loops measured while indenting the same sample spot to the same $|h_{\min}|$ always overlapped. We therefore exclude material damage as a plausible cause of DDH in our experiments.
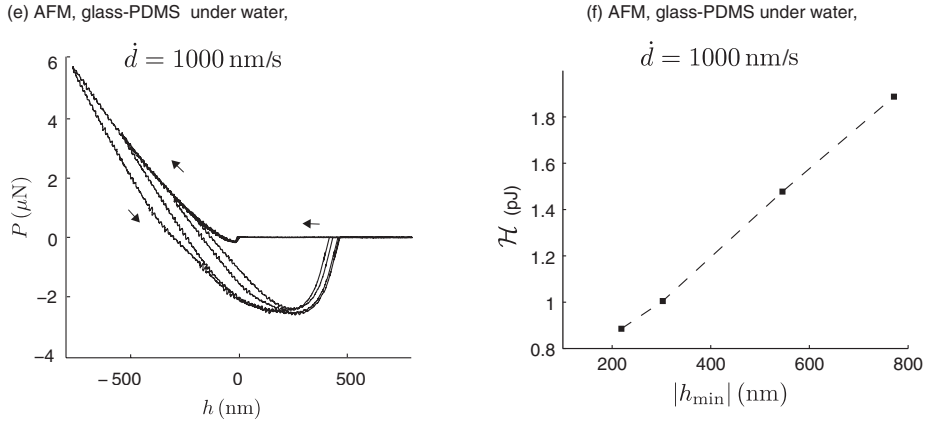
(e) AFM, glass-PDMS under water,

$$\dot{d} = 1000\,\mathrm{nm/s}$$

(f) AFM, glass-PDMS under water,

$$\dot{d} = 1000\,\mathrm{nm/s}$$

Figure 1. Continued.

(a) AFM in air,
$\dot{d} = 1000\,\mathrm{nm/s}$

Spherical tip

PDMS

$|h_{\min}|\,(\mathrm{nm}) = 1500$

Small roughness

1300

1100

Large roughness

(b) NI in air,
$\dot{d} = 1000\,\mathrm{nm/s}$

Flat tip

PDMS

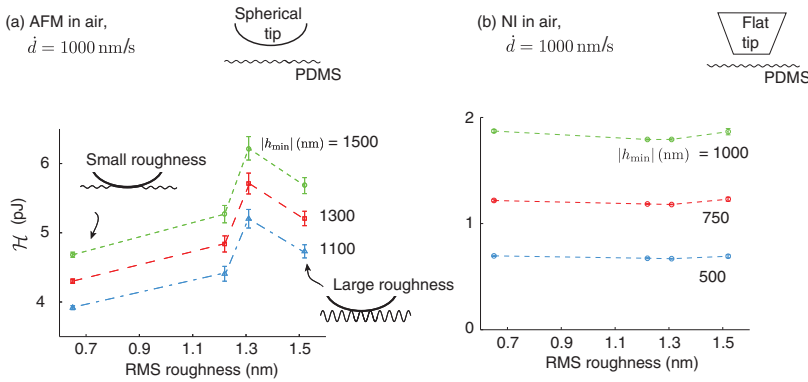$|h_{\min}|\,(\mathrm{nm}) = 1000$

750

500

Figure 2. Energy loss $\mathcal{H}$ on different PDMS samples versus the Si mold roughness on which the PDMS samples were cast, measured using (a) AFM and (b) NI apparatus. The different curves correspond to different $|h_{\min}|$. For each $|h_{\min}|$, the $\mathcal{H}$ for a sample is the average of the data taken over five different locations separated by at least 200 μm. The error bars for $\mathcal{H}$ are the standard deviation of the data taken over the five locations. The error bars in (b) are not clearly visible as there are quite small (10^{-2} pJ). The loading rate $\dot{d}$ for both (a) and (b) was 1000 nm/s. The insets in (a) show the qualitative nature of the contact region hypothesized in this work, in the small, and large roughness limits.

3.2. NI experiments

Viscoelasticity of the sample can cause DDH [25]. To test this possibility, we indented our PDMS samples with a flat tip so that the contact area remained constant during the experiment. Flat-faced tips are not standard for an AFM apparatus. However, a NI apparatus (Section 2.4) with flat-faced diamond tips was readily available. Although the glass-PDMS adhesion energy is different from that of diamond-PDMS,[1] when the contact area remains constant, the adhesion energy should not affect the contact forces.

The $|h_{min}|$ depth, indentation rates and size of contact region in the NI experiments were chosen such that bulk deformation and deformation rates in the NI and AFM experiments were comparable. The $|h_{min}|$ in both the AFM and the NI experiments lay in the range of $\sim$250–1500 nm. The contact area in the NI experiments remained constant at 47 μm^2, while that in the AFM experiments varied from 10 to 230 μm^2 as h went from 0 to 1000 nm. The loading rates, $\dot{d}$, in both AFM and NI experiments were varied in the range $10 - 1000$ nm/s. However note that the base-tip stiffness in the NI experiments is effectively infinite compared to the stiffness of the AFM cantilever. Thus, the deformation rates in the NI experiments are expected to be somewhat larger than those in the AFM experiments for the same $\dot{d}$.

At the loading rate $\dot{d} = 10$ nm/s, the P–h measurements from our NI experiments did not display any appreciable hysteresis, with $\mathcal{H} < 0.03$ pJ. At the higher loading rate of $\dot{d} = 1000$ nm/s, hysteresis was observed and was found to increase with $|h_{min}|$. However, this DDH was insensitive to the sample roughness, as shown in Figure 2b. The NI P–h measurements were quite repeatable, i.e., repeatedly indenting a sample spot to the same $|h_{min}|$ gave indistinguishable P–h curves. Thus, material damage can be ruled out as playing any role in these experiments. In addition, before indenting PDMS, indenting polycarbonate samples using the same NI apparatus showed no hysteresis at all. This shows that the NI apparatus did not have any intrinsic hysteresis associated with it. Thus, the DDH seen in the NI experiments is likely due to the viscoelasticity of the PDMS samples.

Since the NI experiments at $\dot{d} = 10$ nm/s showed negligible viscoelasticity effect, the DDH seen in the AFM experiments at the same low loading rate cannot be explained by viscoelasticity. The NI experiments at $\dot{d} = 1000$ nm/s imply that some fraction of the DDH seen in the AFM experiments at this rate is due to PDMS' viscoelasticity. However, since DDH in the NI experiments did not depend on the sample's roughness, a fraction of the DDH seen in the AFM experiments at $\dot{d} = 1000$ nm/s, specifically, the amount that varies with roughness, cannot be explained solely by PDMS' viscoelasticity.

Therefore, our study shows that there is an additional, yet unaccounted, source of DDH in our AFM experiments. Because the primary difference between the AFM and NI experiments is whether the contact area changes or remains fixed, this unaccounted source of DDH suggests a surface-related mechanism that operates when the contact area changes. This hypothesis is reinforced from the observation that $\mathcal{H}$ in the AFM experiments initially increases and then decreases with the sample's roughness. In the next section, we explore this hypothesis in depth by developing an analytic model of adhesive contact that accounts for surface roughness.

3.3. *Theory: a model for adhesive elastic contact between rough surfaces*

The correlation between DDH and surface roughness suggests that DDH may be *explained in terms of surface roughness*, in the absence of all the other aforementioned factors such as moisture, plasticity, viscoelasticity, etc. In the following we develop such a theory, and answer the following two questions. First, how can roughness

cause DDH? Second, why does the energy loss first increase and then decrease with increasing RMS roughness?

To some extent, the effect of roughness on DDH is surprising, since the RMS roughness of the surfaces of the samples and the indenter (a few nm) is significantly smaller than the radius of the contact region in our experiments (2–8.5 μm). In many situations the effect of such small surface perturbations on $\mathcal{H}$ are negligible, such as in the NI experiments in Figure 2b (see also [26]). As we discuss next, however, surface roughness can change how the contact area *evolves* with h, and hence exert a dramatic influence on $\mathcal{H}$ as shown in Figure 2a.

During a slow loading (unloading) process, the contact area grows (decreases) in a way that is always in equilibrium: changes in elastic and interfacial energies induced by small variations of the contact area exactly balance. When the surfaces are perfectly smooth, only one equilibrium contact area exists for each h. However, multiple equilibria can exist if the surfaces are rough. Among these equilibria, those with smaller contact areas are probed while loading, while equilibria with larger contact areas are explored during unloading. This leads to two different P–h curves for the loading and unloading phases, and is sufficient to cause DDH.

To quantify the magnitude of the energy loss due to roughness, we consider the contact between a rigid spherical indenter with radius R and a wavy sample surface with wave length λ and amplitude $2A$ (Figure 3c). The RMS roughness of this model surface is proportional to A. In the following we find that, as A grows, $\mathcal{H}$ increases when A is small, and decreases when A is large, in agreement with our experimental observations.

We first assume that A is small enough such that the contact area between the two bodies is simply connected, i.e, within the contact area the surfaces adhere uniformly leaving no gaps (*small roughness* in Figure 2a). When the surface shape of the sample is an axi-symmetric sinusoid, the equilibrium P–h curve has been analytically derived in [27], Equations (2), (3), in [14].

Examples of this equilibrium P–h curve are shown in Figures 3a and b, as solid gray curves. The equilibrium P–h curve has oscillations, or folds, owing to the sinusoidal topography of the surfaces. In some cases (such as those shown in Figure 3) the oscillations can be so pronounced that multiple values of P appear for each h, each one the consequence of a different equilibrium contact area. This phenomenon has been discussed in [27], and explored experimentally at the macroscale ($\sim 10^{-2}$ m) in [14].

We construct a model for roughness by first deriving asymptotic forms for Equations (2), (3) of [14] and then using them to derive the equations for the *measured P–h* curve. Specifically, as we will show elsewhere, when $\lambda/R \ll 1$ and $A/\lambda \sim O(1)$, the $P(h)$ curve is multiply valued. Consequently, the P–h curve measured in an experiment does not follow the folds of the equilibrium P–h curve, but depends on the loading history (e.g. the thin solid curve in Figure 3a (red online). As λ/R decreases, the folds in Figure 3a get tighter, (see also Figure 3b). Under these conditions, an experimentally measured P–h loop will essentially follow the envelope of the folded analytic curve, given by[2]

$$P(a) = \frac{4E^*}{3R}a^3 - \sqrt{8\pi\gamma E^*}a^{\frac{3}{2}} \pm 2\pi E^* \frac{A}{\lambda^{1/2}}a^{\frac{3}{2}}, \tag{1a}$$
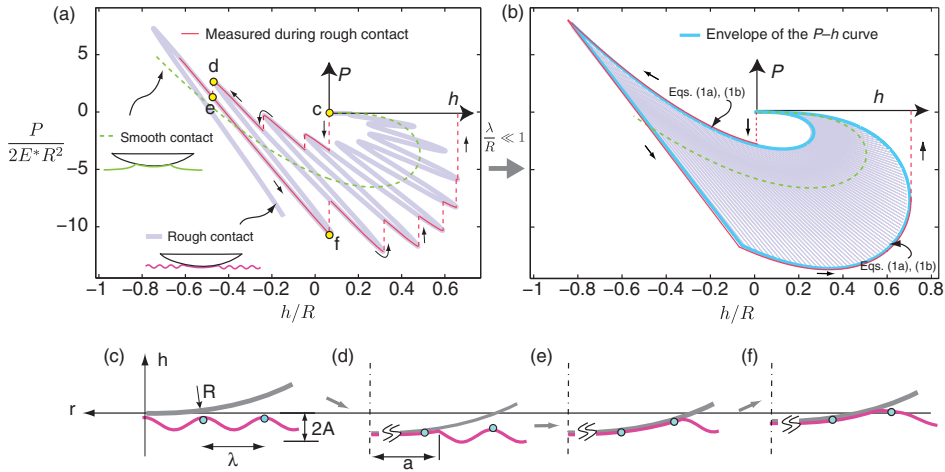
Figure 3. (a) *P–h* curves predicted by a smooth-surface contact model [10] (dashed curve) and by the small roughness contact model studied in this article (thick solid curve). Both curves are parameterized by the radius of the contact area. In an experiment in which *h* is prescribed, sudden changes in the contact area occur at the tip of every fold, such as from *d* to *e*. As a result, an experiment will measure only parts of its envelope (thin solid curve). (b) When the roughness length scale (λ) is much smaller than the radius of the indenter (R) the folds in the *P–h* curve are so close together that the envelope of the *P–h* curve can be described by Equations (1a) and (1b) (thick solid curve). (c)–(f) Contact shapes at different stages of loading/unloading marked in (a).

$$h(a) = \frac{1}{R}a^2 - \sqrt{\frac{2\pi\gamma}{E^*}}a^{\frac{1}{2}} \pm \pi\frac{A}{\lambda^{1/2}}a^{\frac{1}{2}}. \tag{1b}$$

This envelope is parameterized by the radius *a* of the contact area. The shape of the envelope depends on the adhesion energy between the bodies γ and the plain-strain Young's modulus E^*. The + and − signs correspond to the loading and unloading phases of the experiment, respectively. When unloading begins, the experiment will initially sample a leg of the very last fold, which for $\lambda \ll R$ becomes a straight line. An example of the envelope curve is shown in Figure 3b (solid curve (blue online)).

Notice that when $A = 0$, the loading and unloading branches in (1a) and (1b) collapse to a single curve, the equilibrium *P–h* curve given by the JKR contact theory [10]. The JKR theory also considers adhesive contact between a paraboloid and a half-space, but ignores the roughness of the surfaces. Similarly, when both A and γ are set to 0, Equations (1a) and (1b) reduce to the equilibrium *P–h* curve given by Hertz contact theory [11], which ignores both adhesion and roughness.

3.4. *Comparing theory with AFM experiments*

A comparison of the experimental results with a fitting to Equations (1a) and (1b) is shown as dashed lines in Figure 1a. For the fitting we used E^* for PDMS as

0.75 MPa, γ for glass-PDMS contact as 2.6×10^{-2} J and $A/\sqrt{\lambda} = 9 \times 10^{-6}\sqrt{m}$. These values for E^* and γ are very close to the reported values [5,6,28,29] for the same composition of PDMS and glass used in this work (Section 2.2). Additionally, the value of A/λ is commensurate with AFM scans of the glass bead, and the Si mold surfaces, which revealed a combined RMS-roughness of the bead and the samples $\sim$10 nm (A) and features sizes smaller then 1000 nm (λ).

It follows from Equations (1a) and (1b) that $\mathcal{H}$ scales as $(\gamma E^*/\lambda)^{1/2}RA|h_{\min}|$. This means that in the small roughness limit $\mathcal{H}$ increases with the roughness A, $|h_{\min}|$, and adhesion energy γ, all consistent with our experiments. First, Figure 2a shows that $\mathcal{H}$ initially increases with RMS roughness. This finding contrasts the traditional viewpoint in which the pull-off adhesion force decreases with roughness [15]. It may also explain why rolling friction initially increases with roughness, as found by Briggs and Briscoe [30], and first noted in [27]. Second, Figures 1b, d, and f show that $\mathcal{H}$ increases linearly with $|h_{\min}|$ as predicted by our model. Finally, Figures 1c and e show that contact forces under water are larger compared to in air, indicating that the glass-PDMS adhesion energy γ is lower under water.[3] Based on this, our model would predict that the energy loss $\mathcal{H}$ is also lower under water than in air, which is consistent with Figures 1d and f.

We should not expect $\mathcal{H}$ to always increase with A, since for A large enough the contact region ceases to be simply connected. The transition from a simply to a multiply connected contact region for a simpler geometry is known to depend on the parameter $\alpha = \sqrt{\pi^2 A^2 E^*/2\lambda\gamma}$ [26], with the contact region being simply connected for $\alpha < 1$ and multiply connected otherwise. Based on our fitted parameters, we find $\alpha \approx 0.1$. Therefore, it is reasonable to speculate that the change in trend in DDH at the largest roughness shown in Figure 2a is due to a transition from only a few to many patches out of contact within the apparent contact region.

For A large enough, the two bodies are actually in contact only in small patches within the contact region (*large roughness* in Figure 2a, and the elastic interactions among them are negligible. Each patch then attaches/detaches through pullin/pullout instabilities, as predicted by classical contact mechanics theories [10]. The value of $\mathcal{H}$ in this case is determined by the amount of energy lost at each contact patch, times the number of patches. For a sample surface shaped as a sinusoidal egg box, $\mathcal{H}$ scales as[4] $(\lambda/E^*)^{2/3}\gamma^{5/3}RA^{-4/3}|h_{\min}|$. This predicts that $\mathcal{H}$ is of the order of pJ, that it should decrease with A, and that it scales linearly with $|h_{\min}|$, all consistent with our experiments.

4. Conclusions

Our experiments and theoretical model suggest that in some experiments, surface, roughness alone coupled with adhesion can give rise to DDH. A limitation of our work is that we did not have precise control of surface roughness which we could vary only in an average way. For this reason we could not directly measure an effective A or λ for our surfaces. This is important, since it seems unlikely that a single parameter, in this case the RMS roughness, would suffice to completely capture surface topography's effect on the mechanics of contact. Thus, a useful direction to pursue would be to make samples with tailored topographies and then

study the effect of surface topography on contact phenomenon in more detail. Nonetheless, the current study clearly demonstrates that surface topography can give rise to DDH during contact. Our study demonstrates that when there is evidence to suggest that surface roughness is responsible for the observed DDH, then materials properties, such as E^* and γ, can be estimated by simultaneously using both branches of the P–h curve. It is somewhat surprising that while the sample surfaces likely have complicated surface topographies, the fit to Equations (1a) and (1b), which are derived by assuming a sinusoidal surface shape, produces values for the mechanical properties that are in the range of the expected values. These results are encouraging, but further exploration and validation are needed to test the robustness of this procedure to extract mechanical properties from AFM experiments. Our findings also demonstrate the possibility of extracting information about surface roughness at the nanoscale (the value of $A/\sqrt{\lambda}$) even from experiments employing micrometer-sized AFM probes.

Notes

1. In this work, we estimate glass-PDMS adhesion energy to be $26 \, \text{mJ/m}^2$ (Section 3.4). Cao et al. [31] report the diamond-PDMS adhesion energy to be $227 \, \text{mJ/m}^2$. However, from other sources the glass-PDMS adhesion energy is seen to lie in the range 12–$150 \, \text{mJ/m}^2$ [6,32], and the diamond-PDMS adhesion energy is seen to lie in the range 20–$500 \, \text{mJ/m}^2$ [33–35].
2. The derivation of Equations (1a) and (1b) requires considerable space to be properly explained, so it will be published separately. Briey, however, when $\lambda/R \ll 1$ and $A/\lambda \sim O(1)$, the equilibrium P–h curve given by Equations (2), (3) in [14], which are parametric equations of the form $P(a)$, $h(a)$, reduces to a form which contains terms given by the JKR contact theory and additional oscillatory terms arising due to the sinusoidal topography. We derive the equation for the envelope by replacing the oscillatory terms with their respective maximum and minimum values.
3. Reduced adhesion under water has also been observed between mica surfaces [36].
4. The derivation of this expression will be published elsewhere.

References

[1] Y.S. Chu, S. Dufour, J.P. Thiery, E. Perez and F. Pincet, Phys. Rev. Lett. 94 (2) (2005) p.28102.
[2] F.W. DelRio, M.P. de Boer, J.A. Knapp, E.D. Reedy Jr., P.J. Clews and M.L. Dunn, Nature Mater. 4 (2005) p.629.
[3] E.K. Dimitriadis, F. Horkay, J. Maresca, B. Kachar and R.S. Chadwick, Biophys. J. 82 (5) (2002) p.2798.

[4] O. Sahin, S. Magonov, C. Su, C.F. Quate and O. Solgaard, Nature 2 (2007) p.507.
[5] S. Park, M. Goodman and B. Pruitt, Proc. Nat. Acad. Sci. 104 (44) (2007) p.17376.
[6] J. Pickering, D. Van Der Meer and G. Vancso, J. Adhesion Sci. Tech. 15 (12) (2001) p.1429.
[7] N. Maeda, N. Chen, M. Tirrell and J.N. Israelachvili, Science 297 (5580) (2002) p.379.
[8] Y. Chen, C. Helm and J. Israelachvili, J. Phys. Chem. 95 (1991) p.10736.
[9] G. Choi, S. Kim and A. Ulman, Languir 13 (1997) p.6333.
[10] K.L. Johnson, K Kendall and A.D. Roberts, Proc. Roy. Soc. Lon. Ser. A, Math. Phys. Sci. 324 (1558) (1971) p.301.
[11] H. Hertz, J. Reine Angew. Math. 92 (1881) p.156.
[12] B.V. Derjaguin, V.M. Muller and Y.P. Toporov, J. Colloid Interface Sci. 53 (2) (1975) p.314.
[13] D. Maugis, *Contact Adhesion and Rupture of Elastic Solids*, Solid State Sciences, Springer, Berlin, 2000.
[14] P. Guduru and C. Bull, J. Mech. Phys. Solids 55 (3) (2007) p.473.
[15] B. Zappone, K. Rosenberg and J. Israelachvili, Tribology Lett. 26 (3) (2007) p.191.
[16] W. Oliver and G. Pharr, J. Mater. Res. 7 (6) (1992) p.1564.
[17] J. Grobelny, N. Pradeep, D.I. Kim and Z.C. Ying, Appl. Phys. Lett. 88 (2006) p.091906.
[18] M. Giri, D. Bousfield and W. Unertl, Langmuir 17 (10) (2001) p.2973.
[19] H. She, D. Malotky and M. Chaudhury, Langmuir 14 (11) (1998) p.3090.
[20] Y. Xia and G. Whitesides, Annu. Rev. Mater. Sci. 28 (1) (1998) p.153.
[21] F. Hua, Y. Sun, A. Gaur, M.A. Meitl, L. Bilhaut, L. Rotkina, J. Wang, P. Geil, M. Shim and J.A. Rogers, Nano Lett. 4 (12) (2004) p.2467.
[22] N.A. Burnham, X. Chen, C.S. Hodges, G.A. Matei, E.J. Thoreson, C.J. Roberts, M.C. Davies and S.J.B. Tendler, Nanotechnology 14 (1) (2003) p.1.
[23] B. Bhushan, *Springer Handbook of Nanotechnology*, Springer, Berlin, 2006.
[24] J.C. McDonald, D.C. Duffy, J.R. Anderson, D.T. Chiu, H. Wu, O.J.A. Schueller and G.M. Whitesides, Electrophoresis 21 (1) (1999) p.27.
[25] Y.Y. Lin and C.Y. Hui, J. Polymer Sci. Part B Polymer Phys. 40 (2002) p.772.
[26] K. Johnson, Int. J. Solids Struct. 32 (3) (1995) p.423.
[27] P. Guduru, J. Mech. Phys. Solids 55 (3) (2007) p.445.
[28] F. Schneider, T. Fellner, J. Wilde and U. Wallrabe, J. Micromech. Microeng. 18 (6) (2008) p.065008.
[29] X. Brown, K. Ookawa and J. Wong, Biomaterials 26 (16) (2005) p.3123.
[30] G. Briggs and B. Briscoe, Nature 260 (5549) (1976) p.313.
[31] Y. Cao, D. Yang and W. Soboyejoy, J. Mater. Res. 20 (8) (2005) p.2004.
[32] A. Sofla, E. Seker, J.P. Landers and M.R. Begley, J. Appl. Mech. 77 (2010) p.031007.
[33] C.J. Buchko, M.J. Slattery, K.M. Kozloff and D.C. Martin, J. Mater. Res. 15 (1) (2000) p.231.
[34] L. Bes, K. Huan, E. Khoshdel, M.J. Lowe, C.F. McConville and D.M. Haddleton, Eur. Polymer J. 39 (1) (2003) p.5.
[35] A. Bietsch and B. Michel, J. Appl. Phys. 88 (2000) p.4310.
[36] H. Christenson, J. Phys. Chem. 97 (46) (1993) p.12034.